nature climate change

LETTERS

https://doi.org/10.1038/s41558-019-0667-6

Strong remote control of future equatorial warming by off-equatorial forcing

Malte F. Stuecker[1,2*], Axel Timmermann[1,2], Fei-Fei Jin[3], Cristian Proistosescu[4], Sarah M. Kang[5], Doyeon Kim[5], Kyung-Sook Yun[1,2], Eui-Seok Chung[1,2], Jung-Eun Chu[1,2], Cecilia M. Bitz[6], Kyle C. Armour[6,7] and Michiya Hayashi[3]

The tropical climate response to GHG forcing is spatially non-uniform[1–3]. Even though enhanced equatorial and eastern Pacific warming is simulated by most climate models, the underlying mechanisms—including the relative roles of atmospheric and oceanic feedbacks—remain debated. Here, we use a climate model with idealized CO_2-radiative forcing patterns to show that off-equatorial radiative forcing and corresponding coupled circulation/cloud adjustments are responsible for much of equatorial warming in response to global CO_2 forcing. For equatorial forcing, the atmosphere responds by enhancing atmospheric heat export to the extratropics, an associated strengthening of the ascending Hadley circulation branch and strong negative equatorial cloud feedbacks. These processes together greatly dampen equatorial surface warming. Intensification of the oceanic subtropical cells and increased cold subsurface water upwelling in the eastern tropical Pacific provide an additional negative feedback for surface temperatures. In contrast, applying off-equatorial forcing, the atmosphere responds by exporting less heat from the tropics, Hadley circulation weakening and weaker negative equatorial cloud feedbacks, while the subtropical cells slow down in the ocean. Our results demonstrate a delicate balance in the coupled climate system between remote circulation adjustments and regional feedbacks that create the patterns of future climate change.

Recent decades saw important theoretical advances in our understanding of the tropical- and subtropical-climate response to global CO_2 forcing[1–8]. However, differences seen in trends between observations and models cause ongoing debates about driving mechanisms[8–11]. The relative importance and balance of regional radiative feedbacks[12–18], wind–evaporation–sea-surface temperature feedback[2], meridional heat and moisture transport changes[19], the effect of the ocean circulation[20,21] and spatial patterns in radiative forcing[22] in shaping surface temperature and precipitation patterns remains an open question. Specifically, it is unclear how important local forcing and feedbacks are in comparison to remote processes in determining the equatorial warming amplitude and spatial pattern, especially for the transient adjustment of the climate system over the coming decades during which changes in ocean circulation and heat uptake are a major source of uncertainty.

Here we set out to quantify the contributions of various climate feedbacks to the projected equatorial warming, addressing in particular the question of whether local equatorial feedbacks are controlled primarily by local thermodynamic processes or by remote forcing via dynamic adjustments involving large-scale atmospheric and shallow ocean circulation changes. Our analysis is based on an idealized modelling approach that prescribes spatially varying CO_2 concentrations in (1) an atmospheric general circulation model (AGCM) coupled to a slab ocean model (SOM) and (2) the same AGCM coupled to a dynamic ocean (CPL)[23]. Here, we primarily focus on the transient response simulated by the coupled experiments due to their relevance to projected changes in the next few decades during which the ocean still adjusts to the forcing. In contrast, the SOM experiments show the equilibrium climate response in the absence of ocean circulation changes.

First, we use the Community Earth System Model (CESM)[24] in a fully coupled setting and prescribe an abrupt quadrupling of CO_2 concentrations globally in an ensemble experiment (GLOBAL CPL; see Methods). As expected, the transient (year 11–60 average after the perturbation) ensemble-mean surface temperature response at 2-m reference height (TAS) shows the characteristic enhanced warming in the equatorial band (Fig. 1a). Moreover, we see amplified warming in the equatorial upper-troposphere (Fig. 2a), a strengthening and narrowing of the ascending Hadley circulation branch (Supplementary Table 1 and Fig. 2a,d) and an increase of tropical precipitation (Supplementary Fig. 1c). This response—termed previously deep tropical squeeze—in CESM is largely consistent with the projections of other climate models[8].

When abrupt CO_2 quadrupling is only applied in the equatorial band (EQ: 15° S–15° N; Fig. 1d), we see ensemble-mean equatorial surface warming of only 0.74 °C despite the large local radiative forcing (Fig. 1b), a response that is robust among all individual ensemble members (Fig. 1e and Supplementary Fig. 2) and also seen in the CESM SOM simulation (albeit with a somewhat different spatial pattern and amplitude) with the same forcing structure (EQ SOM; Fig. 1e and Supplementary Figs. 2 and 3). The ascending Hadley circulation branch in EQ CPL shows a strengthening and narrowing (indicated by increased low-level inflow as well as outflow occurring at higher altitude in Fig. 2b and Supplementary Table 1), along with enhanced oceanic heat uptake in the eastern equatorial Pacific (Fig. 3a). A strengthening of the ascending Hadley circulation branch is consistent with increases of the meridional surface temperature (Fig. 1b) and energy (Fig. 1d) gradients in the tropics.

[1]Center for Climate Physics, Institute for Basic Science, Busan, Republic of Korea. [2]Pusan National University, Busan, Republic of Korea. [3]Department of Atmospheric Sciences, University of Hawai'i at Mānoa, Honolulu, HI, USA. [4]Joint Institute for the Study of the Atmosphere and the Ocean, University of Washington, Seattle, WA, USA. [5]School of Urban and Environmental Engineering, Ulsan National Institute of Science and Technology, Ulsan, Republic of Korea. [6]Department of Atmospheric Sciences, University of Washington, Seattle, WA, USA. [7]School of Oceanography, University of Washington, Seattle, WA, USA. *e-mail: stuecker@pusan.ac.kr

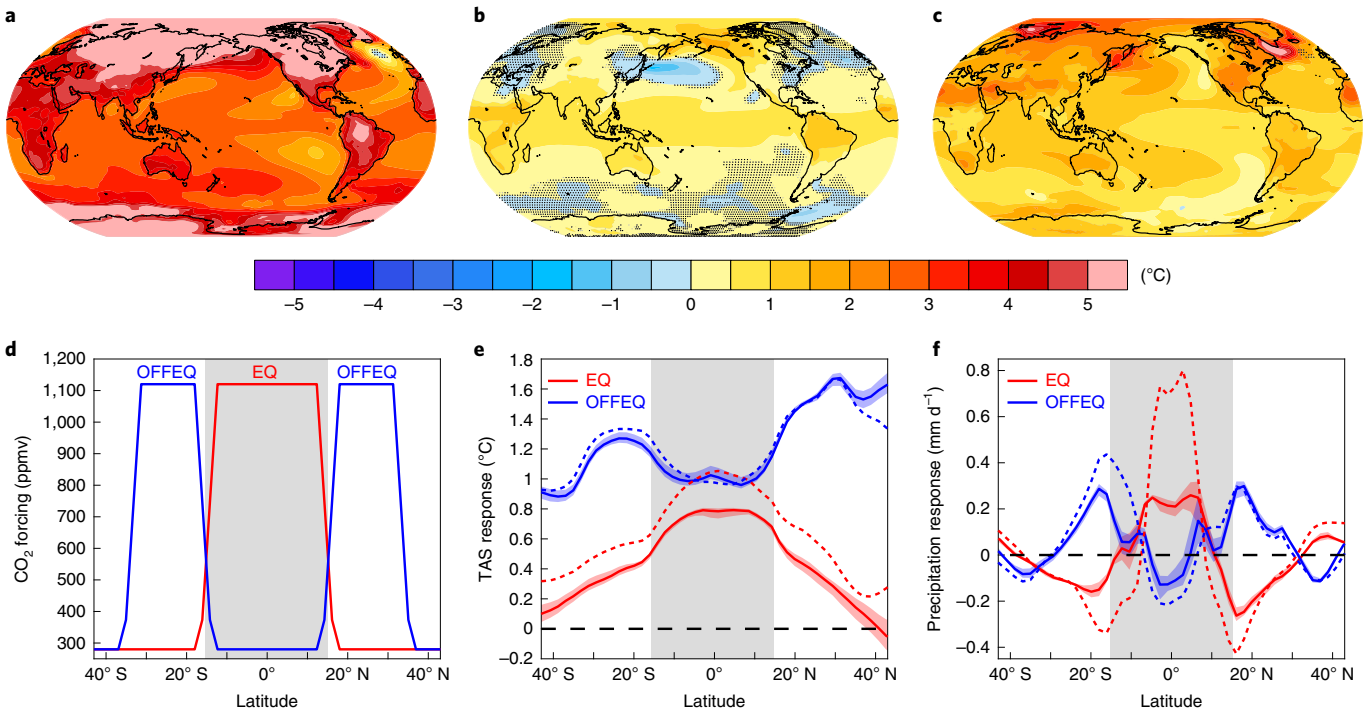

Fig. 1 | Surface temperature and precipitation response to CO_2 forcing. **a**–**c**, TAS response for GLOBAL CPL (**a**), EQ CPL (**b**) and OFFEQ CPL (**c**). Values that are not significantly different from zero at the 95% confidence level are indicated by black stippling (using a local two-tailed *t*-test) and additional grey stippling (using FDR-adjusted critical *P* values). **d**, CO_2 forcing for the EQ and OFFEQ regional forcing experiments. **e**, Zonal-mean TAS response for EQ CPL (solid red), OFFEQ CPL (solid blue), EQ SOM (dashed red) and OFFEQ SOM (dashed blue). **f**, Zonal-mean precipitation (P) response for the same experiments as in **e**. Red and blue shading in **e** and **f** indicates the ensemble range of the responses. Grey shading in **d**–**f** indicates the equatorial region.

In contrast, when CO_2 concentrations are abruptly quadrupled over an equivalent total surface area in the off-equatorial region (OFFEQ: 32°–16° S and 16°–32° N; Fig. 1d), we observe pronounced warming of equatorial TAS (1.02 °C) and throughout the equatorial troposphere despite the absence of local forcing (Fig. 1c), which is again robust among different ensemble members (Fig. 1e and Supplementary Fig. 2) and in a corresponding SOM simulation (OFFEQ SOM; Supplementary Figs. 2 and 3). In OFFEQ CPL, the Hadley circulation slows down (indicated by both decreased low-level inflow and upper-level outflow in Fig. 2c and Supplementary Table 1) and we observe slightly reduced oceanic heat uptake along the Equator (Fig. 3b). Potential mechanisms explaining Hadley circulation weakening include moisture and radiative constraints on vertical velocity[19], direct CO_2-radiative effects[25], a weakening of the meridional surface temperature gradient[26,27] (Fig. 1c) and changes in static stability[9].

Next, by performing additional experiments with mid-latitude (MLAT CPL) and polar (POLAR CPL) CO_2 forcings, we demonstrate that the climate response to regional forcings is largely additive for a 50-yr average (Supplementary Figs. 1 and 4), allowing for a linear decomposition of the climate response[23]. The Hadley circulation response in GLOBAL CPL is mostly the result of a competition between the responses to equatorial (ascending branch strengthening) and off-equatorial (weakening) forcing (Fig. 2a–c and Supplementary Fig. 4a–c). Mid- and high-latitude forcing can act to further weaken and shift the Hadley circulation (Supplementary Fig. 4d,e).

Interestingly, the zonal-mean precipitation responses in the EQ and OFFEQ experiments (both CPL and SOM) are of opposite sign in the tropics and subtropics (Fig. 1f), although both simulations show a warming of the equatorial region (Fig. 1e). A moisture budget analysis (Supplementary Information) reveals that the precipitation increase in the Intertropical Convergence Zone (ITCZ) in response to EQ forcing (in both CPL and SOM) is associated with more convergence of climatological water vapour (Supplementary Figs. 5 and 6), enhanced diabatic forcing and increased vertical motion (negative pressure velocity in Fig. 2e and Supplementary Fig. 3e). The thermodynamic terms (climatological winds transporting more water vapour) do not contribute substantially to the precipitation increase, as the negative contribution from the thermodynamic moisture advection term and the positive contribution from the thermodynamic moisture convergence term nearly cancel each other (Supplementary Figs. 5 and 6).

Correspondingly, the reduction of equatorial precipitation in response to OFFEQ forcing (despite considerable increase in evaporation; Supplementary Figs. 7 and 8) can be explained mostly by decreased convergence of climatological water vapour in this region (in both CPL and SOM), associated with reduced vertical motion (Fig. 2f and Supplementary Fig. 3f) and a weakening of the Hadley circulation (Fig. 2c, Supplementary Figs. 3c and 4b and Supplementary Table 1). While the thermodynamic moisture convergence term contributes to an increase of ITCZ precipitation, it cannot out-compete the larger reduction due to the dynamic moisture convergence term (Supplementary Figs. 7 and 8).

Next, we decompose the contributions to equatorial TAS changes from the energy budget perspective to better understand the reasons for the weak surface warming in EQ. The atmosphere transports heat away (via the dry static energy component[8,19]) from the equatorial region (negative atmospheric heat convergence H_A) for EQ forcing and towards the equatorial region (positive atmospheric heat convergence H_A) for OFFEQ forcing (Fig. 4). These heat transport changes are associated with corresponding changes in Hadley circulation strength discussed earlier. The atmospheric heat transport is larger in SOM compared to CPL (Fig. 4), which can be explained by anomalous negative heat flux from the ocean to the equatorial atmosphere in EQ CPL (and positive in OFFEQ

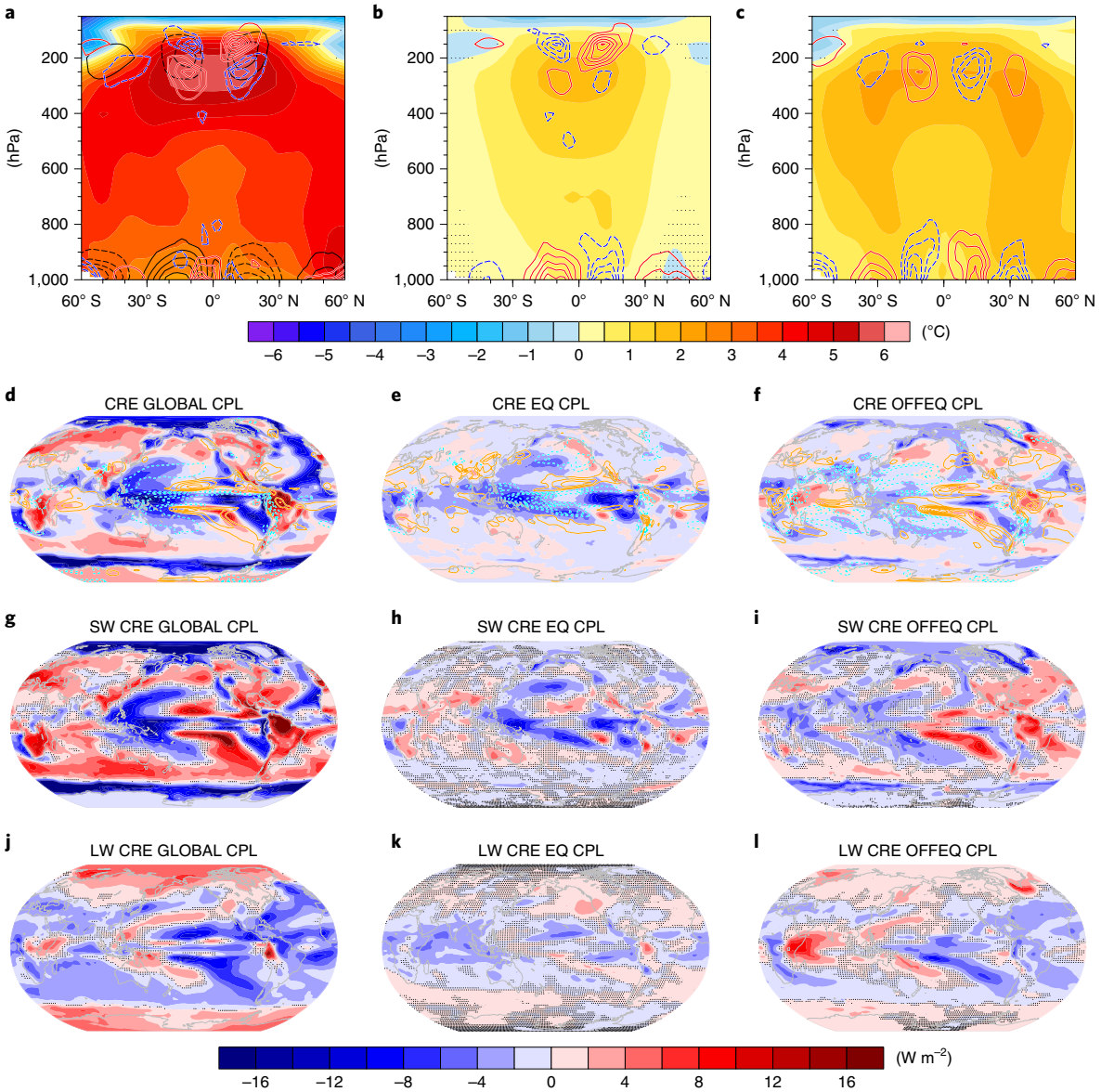

Fig. 2 | Ensemble-mean temperature, meridional wind, vertical pressure velocity and cloud radiative effect (CRE) responses to CO_2 forcing. a–c, Zonal-mean temperature (shading) and meridional wind (coloured contours; solid red indicating positive values and dashed blue negative values) responses for GLOBAL CPL (interval: 0.1 m s^{-1}) (**a**), EQ CPL (interval: 0.05 m s^{-1}) (**b**) and OFFEQ CPL (interval: 0.05 m s^{-1}) (**c**). The climatological zonal-mean meridional wind is overlaid in black contours (interval: 0.5 m s^{-1}) in **a** to indicate the climatological Hadley circulation inflow and outflow. **d–l**, Total CRE (**d–f**), SW CRE (**g–i**) and LW CRE (**j–l**) for GLOBAL CPL (**d**,**g**,**j**), EQ CPL (**e**,**h**,**k**) and OFFEQ CPL (**f**,**i**,**l**). The vertical pressure velocity response at 500 hPa is overlaid in coloured (solid orange for positive values and dashed cyan for negative values) contours (intervals: 0.006 Pa s^{-1} for GLOBAL and 0.003 Pa s^{-1} for EQ and OFFEQ) in **d–f**. Ensemble-mean temperature, SW CRE and LW CRE values that are not significantly different from zero at the 95% confidence level are indicated by black stippling (using a local two-tailed *t*-test) and additional grey stippling (using FDR-adjusted critical *P* values) in **a–c** and **g–l**. Zero contour lines are omitted.

CPL; Figs. 3 and 4) that is absent in SOM (third and fourth columns in Fig. 4). Given these atmospheric and oceanic heat transport adjustments, the overall feedback parameter is greatly reduced in the equatorial band for EQ forcing ($\lambda = -3.51\,W\,m^{-2}\,K^{-1}$ in EQ CPL) compared to OFFEQ forcing ($\lambda = -2.33\,W\,m^{-2}\,K^{-1}$ in OFFEQ CPL), with a large contribution coming from the differences in the cloud response (Fig. 4).

The total (shortwave (SW) + longwave (LW)) cloud radiative effect (CRE) response in GLOBAL is negative in the equatorial band (Fig. 2d and Supplementary Fig. 3d), mostly due to the SW component (Fig. 2g and Supplementary Fig. 3g) in the equatorial Pacific. This negative CRE can largely be explained by the response to local equatorial CO_2 forcing (Fig. 2e,h and Supplementary Fig. 3e,h). In contrast, we see only a weakly negative equatorial CRE in response to OFFEQ forcing (Fig. 2f,i and Supplementary Fig. 3f,i). Thus, the cloud feedback (defined here simply as the equatorial CRE change divided by the equatorial TAS change) is much more negative for EQ forcing compared to OFFEQ forcing (Fig. 4). Importantly, under EQ forcing we see a negative CRE response in the ITCZ and western Pacific warm pool associated with enhanced local ascending motion (Fig. 2e). In addition, we see a negative CRE (mostly due to the SW component) in the eastern tropical Pacific (Fig. 2e,h) due to an increase in low clouds (Supplementary Fig. 9e). Furthermore, the negative LW CRE response to EQ forcing (Fig. 2k) can be mostly explained by a decrease of high clouds in the tropical Indian Ocean (Supplementary Fig. 9h). These results imply that forcing-induced

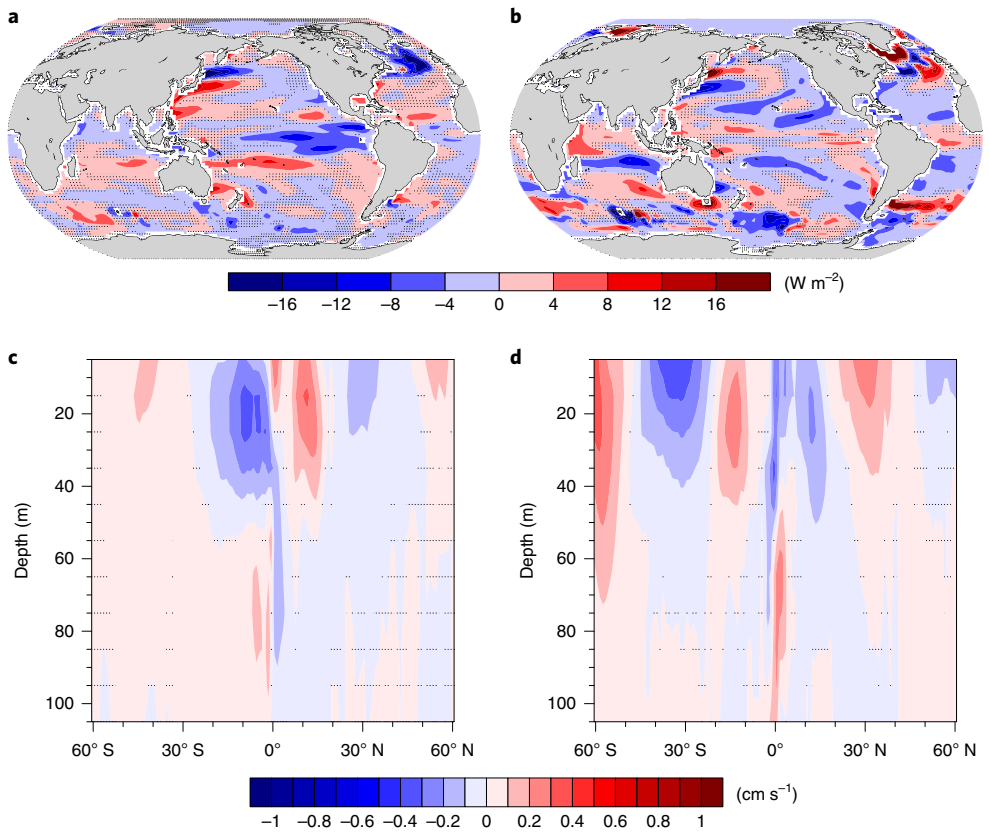

Fig. 3 | Ocean response to CO_2 forcing. a–d, Ensemble-mean net surface heat flux from the ocean to the atmosphere for EQ CPL (**a**) and OFFEQ CPL (**b**), as well as ensemble-mean zonal-mean meridional ocean currents for EQ CPL (**c**) and OFFEQ CPL (**d**). Values that are not significantly different from zero at the 95% confidence level are indicated by black stippling (using a local two-tailed *t*-test) and additional grey stippling (using FDR-adjusted critical *P* values).

Hadley circulation adjustments not only cause atmospheric meridional heat transport changes but also trigger different cloud feedbacks (Fig. 4).

While, in general, we find similarity in the zonal-mean climate response between the CPL and SOM experiments (Figs. 1,4), there is also a major role for the ocean (via its general circulation and associated spatial patterns of heat uptake) to mediate the equatorial surface temperature response during the transient adjustment of the climate system[20], resulting in zonal asymmetries (such as the east–west sea-surface temperature gradient in the tropical Pacific) of the warming pattern (comparing EQ CPL and EQ SOM in Supplementary Fig. 2). As stated earlier, we see anomalous net surface heat flux into the eastern equatorial Pacific ocean in EQ CPL (Fig. 3a), which is explained by enhanced upwelling of subsurface waters (that have not warmed yet via radiative forcing) along the Equator in association with an increased oceanic subtropical cell circulation (Fig. 3c and Supplementary Fig. 10a), resulting in reduced cold-tongue warming. The strength of the subtropical cell is controlled partly by the magnitude of the trade wind circulation[28], thereby linking the Hadley circulation response to changes in equatorial ocean heat uptake (Fig. 4) and the zonal sea-surface temperature gradient. In contrast, in OFFEQ CPL we see slightly decreased net surface heat flux into the equatorial ocean (Fig. 3b) due to reduced cold water upwelling along the Equator and a weaker subtropical cell (Fig. 3d and Supplementary Fig. 10b). Importantly, the CRE spatial patterns (Fig. 2d–l and Supplementary Fig. 3d–l) are shaped by both atmospheric and oceanic circulation adjustments.

Summarizing, while EQ forcing results in an increase of the meridional temperature gradient in the tropics, OFFEQ forcing results in a decrease thereof. However, the equatorial warming magnitude is even larger for OFFEQ forcing than for EQ forcing. The dynamic Hadley circulation changes identified here (Fig. 4) show a first-order control on equatorial radiative feedbacks (especially CRE) in response to forcing, in addition to controlling atmospheric heat transport. The Hadley circulation strength changes also depend on the TAS response, such that the ultimate amount of equatorial heating required to close the energy budget is determined by dynamics that affect the surface as well as the top-of the-atmosphere (TOA) radiation response (radiative feedbacks). For example, the Hadley circulation changes are coupled to the strength of the oceanic subtropical cells[21,28], which control equatorial upwelling[29] and thus both cloud and TAS response patterns. Our results highlight that adjustments of the coupled Hadley circulation/subtropical cell system play a key role in (1) mediating off-equatorial warming into the equatorial region and (2) reducing equatorial warming in response to equatorial radiative forcing (Fig. 4). Thus, the connected Hadley circulation/subtropical cell system can be viewed as a coupled dynamic thermostat.

Moreover, we propose that the Hadley circulation response in traditional experiments with global CO_2 forcing could be interpreted in terms of competing effects between remote and local radiative forcing and their opposing effects on equatorial radiative feedbacks (Supplementary Fig. 4). As cloud feedbacks differ greatly among models and are the largest source of uncertainty in radiative feedback magnitude[18], we would expect the exact balance of this compensation to differ considerably between models. However, we have confidence in the strong control of remote forcing on equatorial temperatures, given that previous aquaplanet simulations with different models showed qualitatively similar zonal-mean TAS responses[30–32]. For instance, a dominant off-equatorial control can

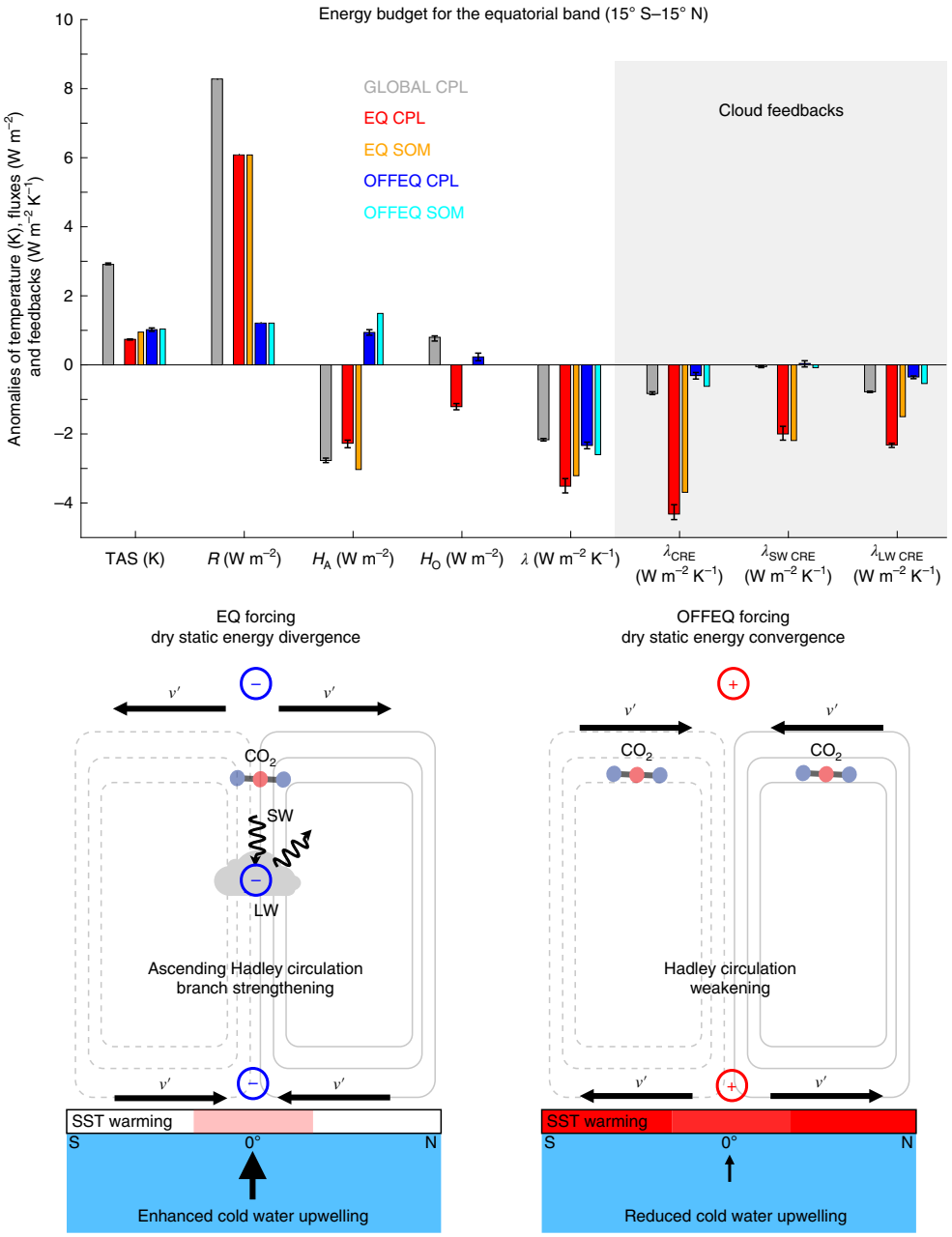

Fig. 4 | Feedback mechanism. Top, Anomalies of TAS, effective radiative forcing (R), net heat flux from the ocean to the atmosphere (H_O), heat convergence due to atmospheric heat transport (H_A), the total feedback parameter (λ), as well as the total (λ_{CRE}), SW ($\lambda_{SW\ CRE}$) and LW ($\lambda_{LW\ CRE}$) cloud feedbacks for the equatorial band. Error bars indicate the ensemble range of the responses and the calculated feedback for the coupled experiments. Bottom, Schematic summary of the physical processes explaining the differing surface temperature response to EQ (left) and OFFEQ (right) forcing where v' is the anomalous zonal-mean meridional wind in the upper and lower troposphere.

also be seen in aquaplanet simulations with the Geophysical Fluid Dynamics Laboratory (GFDL) atmospheric model v.2 (AM2)[31] (Supplementary Table 2).

However, we emphasize that a quantitative assessment of the importance of remote and local forcing for equatorial warming in the coupled climate system (including interactive ocean, ice and land processes) was not possible in previous studies due to the idealized nature of aquaplanets. For instance, our aquaplanet simulation strongly overestimates the negative equatorial feedback in response to EQ forcing compared to the CPL and SOM experiments (comparing Fig. 4 and Supplementary Table 2). As shown by our analysis, the transient warming that will occur over the next decades will be governed mainly by coupled feedbacks between Hadley circulation, clouds and the upper-ocean circulation. Given, for instance, the spatially heterogenous nature of changes in clouds (Fig. 2d–l and Supplementary Fig. 9) and ocean heat uptake (Fig. 3), we propose that a realistic coupled climate model configuration is crucial to understand the surface temperature and precipitation pattern formation during this transient period.

Importantly, the proposed dynamic Hadley circulation/cloud/subtropical cell feedback has implications beyond the projected response of the equatorial region to increases in GHG forcing. For instance, extra-tropical volcanic eruptions and regional anthropogenic aerosol emissions might have a larger impact on

equatorial temperature than previously thought. That is, further reductions of anthropogenic aerosols in off-equatorial regions (and hence increased off-equatorial radiative forcing) might contribute substantially to future equatorial warming. Moreover, this dynamic feedback might explain changes in surface temperature patterns and the hydrological cycle in past climate states, similar to what has been suggested for the Pliocene[33]. Finally, the proposed dynamic feedback and its effects on the tropical climate mean state will also affect projected hydroclimate impacts of tropical climate variability such as those associated with the El Niño/Southern Oscillation as they scale with future projected tropical warming[34].

Online content

Any methods, additional references, Nature Research reporting summaries, source data, extended data, supplementary information, acknowledgements, peer review information; details of author contributions and competing interests; and statements of data and code availability are available at https://doi.org/10.1038/s41558-019-0667-6.

Received: 1 July 2019; Accepted: 20 November 2019;
Published online: 13 January 2020

References

1. Liu, Z., Vavrus, S., He, F., Wen, N. & Zhong, Y. Rethinking tropical ocean response to global warming: the enhanced equatorial warming. *J. Clim.* **18**, 4684–4700 (2005).
2. Xie, S.-P. et al. Global warming pattern formation: sea surface temperature and rainfall. *J. Clim.* **23**, 966–986 (2010).
3. Xie, S.-P., Lu, B. & Xiang, B. Similar spatial patterns of climate responses to aerosol and greenhouse gas changes. *Nat. Geosci.* **6**, 828–832 (2013).
4. Chou, C. & Neelin, J. D. Mechanisms of global warming impacts on regional tropical precipitation. *J. Clim.* **17**, 2688–2701 (2004).
5. Seager, R., Naik, N. & Vecchi, G. A. Thermodynamic and dynamic mechanisms for large-scale changes in the hydrological cycle in response to global warming. *J. Clim.* **23**, 4651–4668 (2010).
6. Ma, J. & Xie, S.-P. Regional patterns of sea surface temperature change: a source of uncertainty in future projections of precipitation and atmospheric circulation. *J. Clim.* **26**, 2482–2501 (2013).
7. Vallis, G. K., Zurita-Gotor, P., Cairns, C. & Kidston, J. Response of the large-scale structure of the atmosphere to global warming. *Q. J. R. Meteorol. Soc.* **141**, 1479–1501 (2014).
8. Lau, W. K. M. & Kim, K.-M. Robust Hadley circulation changes and increasing global dryness due to CO_2 warming from CMIP5 model projections. *Proc. Natl Acad. Sci. USA* **112**, 3630–3635 (2015).
9. Chemke, R. & Polvani, L. M. Opposite tropical circulation trends in climate models and in reanalyses. *Nat. Geosci.* **12**, 528–532 (2019).
10. Seager, R. et al. Strengthening tropical Pacific zonal sea surface temperature gradient consistent with rising greenhouse gases. *Nat. Clim. Change* **9**, 517–522 (2019).
11. Chung, E.-S. et al. Reconciling opposing Walker circulation trends in observations and model projections. *Nat. Clim. Change* **9**, 405–412 (2019).
12. Soden, B. J. & Held, I. M. An assessment of climate feedbacks in coupled ocean–atmosphere models. *J. Clim.* **19**, 3354–3360 (2006).
13. Armour, K. C., Bitz, C. M. & Roe, G. H. Time-varying climate sensitivity from regional feedbacks. *J. Clim.* **26**, 4518–4534 (2013).
14. Rose, B. E. J., Armour, K. C., Battisti, D. S., Feldl, N. & Koll, D. D. B. The dependence of transient climate sensitivity and radiative feedbacks on the spatial pattern of ocean heat uptake. *Geophys. Res. Lett.* **41**, 1071–1078 (2014).
15. Voigt, A. & Shaw, T. A. Circulation response to warming shaped by radiative changes of clouds and water vapour. *Nat. Geosci.* **8**, 102–106 (2015).
16. Feldl, N. & Bordoni, S. Characterizing the Hadley circulation response through regional climate feedbacks. *J. Clim.* **29**, 613–622 (2016).
17. Ceppi, P. & Hartmann, D. L. Clouds and the atmospheric circulation response to warming. *J. Clim.* **29**, 783–799 (2016).
18. Ceppi, P., Brient, F., Zelinka, M. D. & Hartmann, D. L. Cloud feedback mechanisms and their representation in global climate models. *WIREs Clim. Change* **8**, e465 (2017).
19. Held, I. M. & Soden, B. J. Robust responses of the hydrological cycle to global warming. *J. Clim.* **19**, 5686–5699 (2006).
20. Clement, A. C., Seager, R., Cane, M. A. & Zebiak, S. E. An ocean dynamical thermostat. *J. Clim.* **9**, 2190–2196 (1996).
21. Chemke, R. & Polvani, L. M. Ocean circulation reduces the Hadley cell response to increased greenhouse gases. *Geophys. Res. Lett.* **45**, 9197–9205 (2018).
22. Xia, Y. & Huang, Y. Differential radiative heating drives tropical atmospheric circulation weakening. *Geophys. Res. Lett.* **44**, 10592–10600 (2017).
23. Stuecker, M. F. et al. Polar amplification dominated by local forcing and feedbacks. *Nat. Clim. Change* **8**, 1076–1081 (2018).
24. Gent, P. R. et al. The community climate system model version 4. *J. Clim.* **24**, 4973–4991 (2011).
25. Merlis, T. M. Direct weakening of tropical circulations from masked CO_2 radiative forcing. *Proc. Natl Acad. Sci. USA* **112**, 13167–13171 (2015).
26. Gastineau, G., Li, L. & LeTreut, H. The Hadley and Walker circulation changes in global warming conditions described by idealized atmospheric simulations. *J. Clim.* **22**, 3993–4013 (2009).
27. Seo, K.-H., Frierson, D. M. W. & Son, J.-H. A mechanism for future changes in Hadley circulation strength in CMIP5 climate change simulations. *Geophys. Res. Lett.* **40**, 5251–5258 (2014).
28. Nonaka, M., Xie, S.-P. & McCreary, J. P. Decadal variations in the subtropical cells and equatorial Pacific SST. *Geophys. Res. Lett.* **29**, 20-1–20-4 (2002).
29. McCreary, J. P. & Lu, P. Interaction between the subtropical and equatorial ocean circulations: the subtropical cell. *J. Phys. Oceanogr.* **24**, 466–497 (1994).
30. Kang, S. M. & Xie, S.-P. Dependence of climate response on meridional structure of external thermal forcing. *J. Climate* **27**, 5593–5600 (2014).
31. Kang, S. M., Park, K., Jin, F.-F. & Stuecker, M. F. Common warming pattern emerges irrespective of forcing location. *J. Adv. Model. Earth Sys.* **9**, 2413–2424 (2017).
32. Shaw, T. A. & Tan, Z. Testing latitudinally dependent explanations of the circulation response to increased CO_2 using aquaplanet models. *Geophys. Res. Lett.* **45**, 9861–9869 (2018).
33. Burls, N. J. & Fedorov, A. V. Wetter subtropics in a warmer world: contrasting past and future hydrological cycles. *Proc. Natl Acad. Sci. USA* **114**, 12888–12893 (2017).
34. Cai, W. et al. Increasing frequency of extreme El Niño events due to greenhouse warming. *Nat. Clim. Change* **4**, 111–116 (2014).

Methods

Model experiments. The CESM v.1.2.2 (ref. [24]) with the finite volume community atmosphere model v.4 (CAM4)[35] is used to conduct a hierarchy of simulations with idealized CO_2 concentrations abruptly quadrupled either regionally or globally. The atmosphere (26 vertical levels) and land have a nominally 2° horizontal resolution and ocean (60 vertical levels) and sea-ice have a nominally 1° horizontal resolution.

Both CPL and SOM experiments were conducted. The CPL simulations were initialized from year 901 of a fully coupled pre-industrial control simulation at a quasi-equilibrated ocean state. Five ensemble members (with perturbed initial conditions) were used for each experiment: (1) equatorial (EQ CPL) regional forcing (abruptly quadrupled CO_2 prescribed between 15° S and 15° N), (2) off-equatorial (OFFEQ CPL) regional forcing (abruptly quadrupled CO_2 prescribed between 32°–16° S and 16°–32° N), (3) mid-latitude (MLAT CPL) regional forcing (abruptly quadrupled CO_2 prescribed between 59°–33° S and 33°–59° N), (4) polar (POLAR CPL) regional forcing (abruptly quadrupled CO_2 prescribed between 90°–60° S and 60°–90° N) and (5) globally uniform abrupt CO_2 quadrupling (GLOBAL CPL). We mostly focus on the comparison between the EQ and OFFEQ experiments, for which the total forcing area is approximately the same, covering about 25% of the global surface area for each case. A 50-yr average (model years 11–60) of the coupled control simulation (CTRL CPL) is the reference climate for the coupled experiments. The climatological Q-fluxes[36] are calculated from this control and used to generate the reference climate (CTRL SOM) for a suite of SOM experiments (EQ SOM, OFFEQ SOM and GLOBAL SOM). Except for the CO_2 perturbations we use the standard CESM configurations for both the CPL (B1850 component set) and SOM (E_1850_CN component set but with land biogeochemistry turned off) simulations.

The climate responses in EQ CPL, OFFEQ CPL, MLAT CPL, POLAR CPL and GLOBAL CPL are calculated as the anomalies respective to CTRL CPL using 50-yr averages (years 11–60) of each ensemble member. We refer to this time-average as a 'transient response' as the ocean heat uptake and surface temperature have not yet equilibrated with the prescribed forcing. The ensemble spread is relatively small as the time averages are sufficiently long (Supplementary Fig. 2). By contrasting the response in the CPL and SOM experiments, we determine the influence of anomalous ocean heat uptake and transport on the surface climate response. Each SOM experiment is integrated for 120 yr and time averages of the last 90 yr (31–120) are calculated. More details on a similar experimental setup can be found in Stuecker et al.[23]. It was demonstrated in their study that the climate response in similar experiments is spatially linear, that is, the responses to local forcing (that span the total global area) sum approximately to the response to global forcing[23]. This linearity also holds for the experiments presented in this study (Supplementary Figs. 1 and 4). Moreover, 50-yr time averages are sufficiently long to ensure small differences between ensemble members[23].

We conducted AGCM experiments with the sea-surface temperature and sea-ice concentration climatologies calculated from the 60-yr average of the CTRL CPL experiment to generate the boundary conditions for additional AGCM experiments. A control (CTRL AGCM) and three perturbation experiments (GLOBAL AGCM, EQ AGCM and OFFEQ AGCM) were run with the same CO_2 forcing structures (Fig. 1d). Each experiment is run for 60 yr and the last 50 yr (years 11–60) are used to calculate time averages. The anomalies for these experiments are respective to CTRL AGCM. The TOA radiative imbalance diagnosed from these experiments is used to calculate the effective radiative forcing[23], following the radiative forcing model intercomparison project (RFMIP) protocol[37], for each prescribed CO_2 pattern (Fig. 4).

Finally, we performed additional experiments using the same EQ and OFFEQ forcing latitudes using an aquaplanet configuration of the GFDL AM2 (ref. [38]) model. However, instead of prescribing a CO_2 perturbation, we introduced an anomalous surface heat flux of 6 W m^{-2} (similar to the configuration in Kang et al.[31]) over the EQ and OFFEQ regions respectively. We used annual-mean insolation and a uniform mixed layer depth of 10 m. The climate response is averaged over 40-yr simulation after a 10-yr spin-up (Supplementary Table 2). These experiments were conducted to show model robustness that equatorial warming is strongly controlled by remote off-equatorial forcing, even when we are missing crucial land and ocean processes. However, we emphasize that a prescribed surface radiative forcing also neglects the direct CO_2 effect on the circulation[25,39], which in contrast is present in the CESM experiments with prescribed CO_2 forcing.

Black stippling in all figures indicates that ensemble-mean values of the respective variable displayed in shading are not significantly different from zero at the 95% confidence level (using a local two-tailed t-test criterium). Values that are additionally not significantly different from zero using more conservative false discovery rate (FDR) adjusted critical P values[40,41] with a control level of 90% (appropriate for moderate and strong spatial correlation; see discussion in Wilks[41]) are indicated by additional grey stippling.

Feedback calculation. We approximate the anomalous energy balance for the equatorial band (averaged from 15° S–15° N) in the following form[23]:

$$\lambda = -(R + H_A + H_O)/\mathrm{TAS} \quad (1)$$

where the feedback parameter λ is calculated from the effective radiative forcing R (the net TOA radiative imbalance diagnosed from the AGCM simulations), the net heat flux anomalies from the ocean to the atmosphere H_O, the anomalous heat convergence due to atmospheric heat (including both the dry and moist static energy components) transport H_A (calculated by the difference between TOA radiative imbalance and the absorbed net surface heat flux changes in each experiment) and the near-surface air temperature anomaly at the 2-m reference height response TAS.

The effective radiative forcing (as calculated via the standard RFMIP protocol[37]) contains minor contributions from adjustments of water vapour, clouds and temperatures associated with land and sea-ice warming. These are sometimes considered fast feedback processes. Correspondingly, our feedback parameter (Fig. 4) includes very small contributions from temperature and tropospheric water vapour changes in the AGCM experiments that are sometimes considered part of the forcing[23].

We estimate the total cloud feedback, as well as the shortwave and longwave components, by dividing the total CRE, SW CRE and LW CRE averaged in the equatorial band by the equatorial TAS response (Fig. 4). This calculation does not include any corrections that are sometimes used (see discussion in ref. [12]). Nevertheless, it estimates the cloud feedback strength reasonably well (see for instance discussion in ref. [42]).

Data availability

The data from the regionally forced model simulations are available on the IBS Center for Climate Physics climate data server (https://climatedata.ibs.re.kr/).

Code availability

The CESM source code can be obtained from http://www.cesm.ucar.edu/models/cesm1.2/ and the code modifications[43] that allow prescribing spatially varying CO_2 concentrations can be obtained from https://github.com/stuecker/regionalCO2/.

References

35. Neale, R. B. et al. The mean climate of the community atmosphere model (CAM4) in forced SST and fully coupled experiments. *J. Clim.* **26**, 5150–5168 (2013).
36. Bitz, C. M. et al. Climate sensitivity of the community climate system model, version 4. *J. Clim.* **25**, 3053–3070 (2012).
37. Pincus, R., Forster, P. M. & Stevens, B. The radiative forcing model intercomparison project (RFMIP): experimental protocol for CMIP6. *Geosci. Model Dev.* **9**, 3447–3460 (2016).
38. Anderson, J. L. et al. The new GFDL global atmosphere and land model AM2-LM2: evaluation with prescribed SST simulations. *J. Clim.* **17**, 4641–4673 (2004).
39. Bony, S. et al. Robust direct effect of carbon dioxide on tropical circulation and regional precipitation. *Nat. Geosci.* **6**, 447–451 (2013).
40. Ventura, V., Paciorek, C. J. & Risbey, J. S. Controlling the proportion of falsely rejected hypotheses when conducting multiple tests with climatological data. *J. Clim.* **17**, 4343–4356 (2004).
41. Wilks, D. S. The stippling shows statistically significant grid points: how research results are routinely overstated and overinterpreted, and what to do about it. *BAMS* **97**, 2263–2273 (2016).
42. Medeiros, B., Stevens, B. & Bony, S. Using aquaplanets to understand the robust responses of comprehensive climate models to forcing. *Clim. Dynam.* **44**, 1957–1977 (2015).
43. Stuecker, M. F. stuecker/regionalCO2: beta (Version v1.0). Zenodo http://doi.org/10.5281/zenodo.3541484 (2019).

Acknowledgements

M.F.S., A.T., K.-S.Y., J.-E.C. and E.-S.C. were supported by the Institute for Basic Science (project code IBS-R028-D1). F.-F.J. was supported by NSF grant no. AGS?1813611 and DOE grant no. DE-SC0005110. C.M.B. was supported by NOAA grant no. CPO NA115OAR4310161. C.P. was supported by a JISAO postdoctoral fellowship. K.C.A. was supported by NSF grant no. AGS-1752796. S.M.K. and D.K. were supported by Basic Science Research Program through the National Research Foundation of Korea funded by the Ministry of Science, ICT and Future Planning (grant no. 2016R1A1A3A04005520). M.H. was supported by JSPS Overseas Research Fellowships (no. 201860671). Computing resources were provided by University of Southern California's Center for High-Performance Computing. M.F.S. thanks S.-P. Xie and A. N. Babu for valuable discussions.

Author contributions

M.F.S. designed the study and wrote the initial manuscript draft. M.F.S. and D.K. conducted the model experiments and performed the analysis. All authors contributed to the interpretation of the results and to the improvement of the manuscript.

Competing interests

The authors declare no competing interests.

Additional information

Supplementary information is available for this paper at https://doi.org/10.1038/s41558-019-0667-6.

Correspondence and requests for materials should be addressed to M.F.S.

Reprints and permissions information is available at www.nature.com/reprints.